2nd Advanced Optical Metrology Compendium

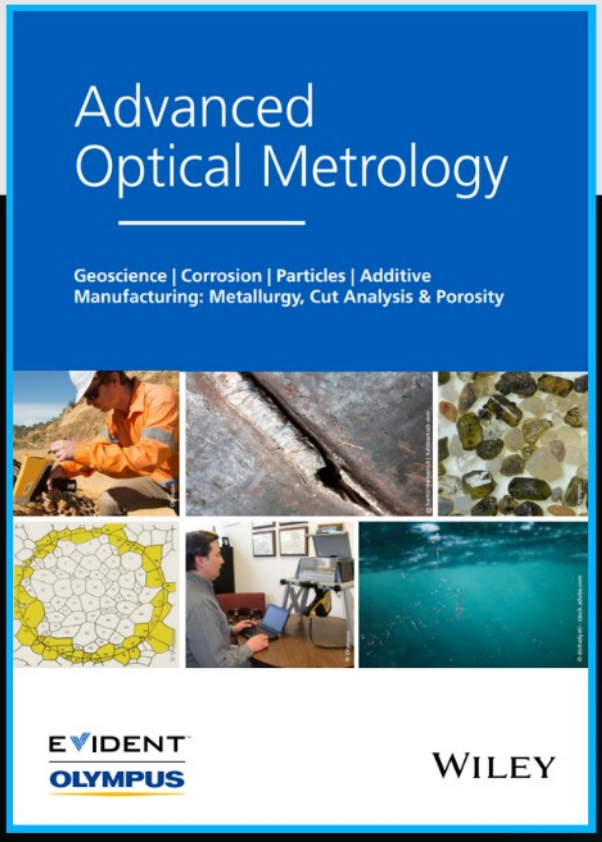

The latest eBook from Advanced Optical Metrology. Download for free.

This compendium includes a collection of optical metrology papers, a repository of teaching materials, and instructions on how to publish scientific achievements.

With the aim of improving communication between fundamental research and industrial applications in the field of optical metrology we have collected and organized existing information and made it more accessible and useful for researchers and practitioners.

EVIDENT
OLYMPUS

WILEY

ADVANCED FUNCTIONAL MATERIALS
www.afm-journal.de

Engineering Micropatterned Dry Adhesives: From Contact Theory to Handling Applications

René Hensel, Karsten Moh, and Eduard Arzt*

Reversible adhesion is the key functionality to grip, place, and release objects nondestructively. Inspired by nature, micropatterned dry adhesives are promising candidates for this purpose and have attracted the attention of research groups worldwide. Their enhanced adhesion compared to nonpatterned surfaces is frequently demonstrated. An important conclusion is that the contact mechanics involved is at least as important as the surface energy and chemistry. In this paper, the roles of the contact geometry and mechanical properties are reviewed. With a focus on applications, the effects of substrate roughness and of temperature variations, and the long-term performance of micropatterned adhesives are discussed. The paper provides a link between the current, detailed understanding of micropatterned adhesives and emerging applications.

1. Introduction

Adhesion—the mutual attraction of objects in contact—is a universal phenomenon exhibited by nearly all classes of matter. In the course of biological evolution, solutions for controlling adhesion have evolved, e.g., for allowing organisms to temporarily or permanently attach to solids in various environments. Such natural solutions exist for standard ambient conditions, for high and low temperatures, for variable humidity and even for underwater conditions. Transferring these concepts into engineering solutions is currently underway to create new mechanical devices, especially in the field of automation and robotics.

Reversible or switchable adhesives are of particular fascination for research groups worldwide. Reversibility enables repeated cycles of attachment and detachment without damaging the contact between the adhering objects or the objects themselves. In nature, the most exciting examples of such reusable adhesives are the fibrillar foot pad organs of insects, spiders, and lizards. They are designated for locomotion over various types of substrates, involving attachment and detachment within milliseconds.[1–5] It is of interest for evolutionary biologists that many foot pads are strikingly similar in morphology: elongated fibrillar structures with aspect ratios ranging from 10 to 80 leading to terminal elements with very different shapes (**Figure 1**a and Figure 3).[6–9] For some animals such as the gecko, the adhesive ability of their toe pads can be attributed to van der Waals interactions and, to some extent, to capillary forces.[10–15] In the gecko, the fibrillar pads are composed of millions of keratinous hairs (called *setae*) that branch into even finer terminal elements (*spatulae*) (Figure 1a).[16,17] Such a hierarchically organized structure results in a soft and compliant surface, which allows easy adaption to roughness at the expense of little strain energy and thus enhances adhesion.

More than 1000 reports published in the field of bioinspired dry adhesives over the last two decades reflect a considerable interest in resolving the underlying adhesion mechanisms, e.g., refs. [18–21]. Application-oriented publications were motivated by a strong interest in creating novel gripper devices and pick-and-place systems (Figure 1b), e.g., refs. [18–20] and [22–24], climbing robots for terrestrial and extraterrestrial activities,[25–32] new gasket designs in microfluidics,[33,34] or novel solutions for biomedical applications.[35–38]

The present feature article aims to describe the path from fundamental considerations, including a detailed understanding of the relevant contact mechanics, to emerging applications. It is now known that the success of mimicking micropatterned dry adhesives critically depends on the interplay between design parameters, such as dimensions of the structure elements and the terminal tip-shape geometry, and the bulk and surface properties of the materials in contact. How these parameters control the adhesive performance of synthetic micropatterned adhesives is reviewed in Section 2. In Section 3, we report on the present state-of-the-art of resulting applications, including, e.g., concepts for switchability and the long-term performance of such structures. In Section 4, relevant operating conditions pertaining to substrate roughness and temperature are discussed. A summary and future perspectives conclude the paper in Section 5.

2. Principles of Adhesive Micropatterns

The governing principle of fibrillar dry adhesives rests on the observation that discrete or micropatterned surfaces typically

Dr. R. Hensel, Dr. K. Moh, Prof. E. Arzt
INM – Leibniz Institute for New Materials
Campus D2 2, Saarbrücken 66123, Germany
E-mail: rene.hensel@leibniz-inm.de
Prof. E. Arzt
Department of Materials Science and Engineering
Saarland University
Campus D2 2, Saarbrücken 66123, Germany
The ORCID identification number(s) for the author(s) of this article can be found under https://doi.org/10.1002/adfm.201800865.

DOI: 10.1002/adfm.201800865

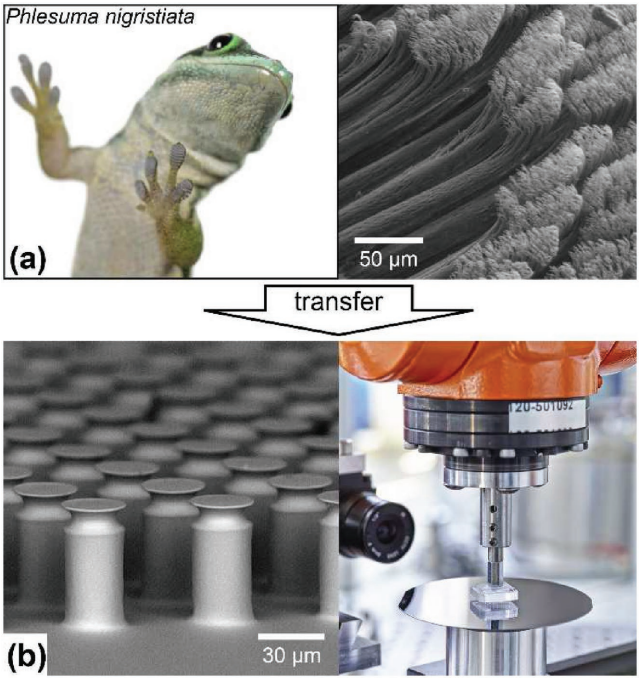

Figure 1. Micropatterned dry adhesives in nature and their transfer to synthetic handling solutions. a) The hierarchical adhesive structure of a gecko toe (*Phlesuma nigristiata*, left) containing hundreds of thousands of setae. Scanning electron image showing setae branching into finer spatular structures (right). b) Scanning electron image of synthetic micropatterned adhesives shaped from an elastomeric polymer (left). Commercial robot equipped with a micropatterned adhesive demonstrating reversible adhesion for utilization in pick-and-place handling (right).

exhibit higher adhesion than unpatterned, flat adhesives [39,40]— this is frequently referred to as the principle of contact splitting.[2] At first glance, this observation is counterintuitive since patterned surfaces create per se less contact area with a substrate. Consequently, the adhesion force cannot simply scale in proportion with the contact area, even though adhesion is an interface-related phenomenon. Two essential mechanical aspects, which are at the heart of theoretical contact mechanics, must be taken into account:[41,42]

- Elastic strain penalty: an adhesive contact formed between two nonconforming elastic solids (i.e., those whose surfaces do not match perfectly) creates stored elastic strain energy in the bulk of the solids close to the contact area; this energy contribution counteracts adhesion.
- Nonuniform contact stresses: When the two adhering solids are pulled against each other, interfacial stresses evolve across the contact area. Due to edge effects and boundary conditions, the resulting stress distributions will include stress concentrations or singularities. Where such interfacial peak stresses exceed the adhesive interaction between the solids, cracks will initiate and cause detachment.

2.1. The Contact Splitting Effect

Research on contact splitting and its benefits for creating high performance adhesives started in the early years of the millennium. The deduction that the strong gecko adhesion must be based on intrinsically weak van der Waals interactions triggered numerous experimental and theoretical studies.[1] Arzt et al.[2] found a strong correlation between areal density of attachment hairs and body mass of animals as diverse as flies, beetles, spiders, and lizards. An interpretation of this correlation was sought within the framework of the classical Johnson, Kendall, and Roberts (JKR) theory on adhesion of (hemi)spherical objects.[43] A tip radius, R, was assumed to scale in a self-similar manner with animal volume. The adhesion force deduced in this way was proportional to $\sqrt{n} \cdot R$, where n is the number of hairs resulting from splitting up the

René Hensel studied materials science at the TU Dresden, Germany. He was a fellow of the DFG Research Training Group 1401/2 at the TU Dresden and did his doctorate at the Leibniz Institute of Polymer Research Dresden (IPF) and the Max Bergmann Center of Biomaterials Dresden (MBC). Since 2014, he has been deputy head of the Program Division Functional Microstructures at Leibniz Institute for New Materials Saarbrücken, Germany.

Karsten Moh studied physics at the University of Duisburg. He received his doctorate in inorganic chemistry at Saarland University. Since 2003, he has been research scientist at INM, and, intermittently, CEO of the Center of competence for nanochemistry (cc-NanoChem e.V.). In 2014, he joined the Program Division Functional Microstructures at Leibniz Institute for New Materials Saarbrücken, Germany, where he is head for industry transfer and applications.

Eduard Arzt is scientific director and chairman (CEO) of INM and jointly Professor for New Materials at Saarland University. He received a Ph.D. in physics from the University of Vienna, Austria, followed by a post-doctoral period at Cambridge University, UK. He was a group leader and, from 1990 to 2007, director at the Max Planck Institute for Metals Research, Stuttgart, and Professor for Metal Physics at the University of Stuttgart. As visiting professor and researcher, he worked at Stanford University, Massachusetts Institute of Technology, and the University of California.

contact. As the adhesion force scaled with a geometrical length (not an area), it was concluded that the adhesion stress (force per area R^2) would progressively increase for smaller tips. An intuitive explanation for the contact splitting effects lies in a reduction of the elastic strain energy penalty for smaller contacts.[2]

The admittedly crude assumption of spherical contacts (see refs. [6,44], and [45]) was subsequently dropped and similar analyses for different contact shapes are available.[46] They find that, for different contact geometries, the pull-off force of a micropattern with n contacts, F', is related to the pull-off force for a contact without splitting, F, by

$$F' = n^s F \tag{1}$$

where the quantity s is called the "contact splitting efficiency."

Important refinements were introduced by Hui et al., who analyzed the adhesion and the resulting contact splitting effect for cylindrical pillars, i.e., punches with a constant cross-section and a flat face in contact with a flat substrate.[41] In their work, they considered two extreme configurations, i.e., a rigid punch adhering to an elastic substrate and an elastic punch adhering to a rigid substrate. The former was shown to be related to Griffith's theory of fracture mechanics,[47–49] but is not realistic in view of most experimental studies: micropatterned adhesives are usually made from soft elastic polymers (elastic modulus in the range of a few MPa), and typical substrates are much stiffer. In general, the adhesion performance of a flat punch will depend on the interfacial stress distribution, which is in turn affected by the material properties and the frictional and boundary conditions.[50–52]

Here we reiterate the recent treatment, by the Cambridge group, of an elastic flat punch perfectly bonded to a rigid substrate (no-slip condition). The asymptotic solutions for the normal stress component, σ_{22}, and the shear stress component, σ_{12}, near the edge are

$$\begin{aligned}\sigma_{22} &= H_1\, r^{-\lambda}\\ \sigma_{12} &= 0.505 H_1\, r^{-\lambda}\end{aligned} \tag{2}$$

where r is the radial distance from the edge of the punch, H_1 the intensity, and λ the order of the singularity.[52] The intensity of the singularity can be written in terms of the applied axial stress, σ_A, and the diameter of the punch, D, as

$$H_1 = \tilde{a}\,\sigma_A\, D^{\lambda} \tag{3}$$

where $\tilde{a} = 0.278$ (axisymmetric, 3D) and $\tilde{a} = 0.331$ (plane strain, 2D), and $\lambda = 0.406$. For an axisymmetric punch, the normalized interfacial stress components near the edge ($r \to 0$) are

$$\begin{aligned}\frac{\sigma_{22}}{\sigma_A} &= 0.278\left(\frac{r}{D}\right)^{-0.406}\\ \frac{\sigma_{12}}{\sigma_A} &= 0.140\left(\frac{r}{D}\right)^{-0.406}\end{aligned} \tag{4}$$

The interface cannot support the infinite stresses predicted by Equation (4) but a cohesive zone establishes at the edge. The failure of the cohesive zone results in crack initiation which, in turn, leads to crack growth and finally pull-off.

A detailed analysis of the interfacial fracture mechanics was recently published by Fleck et al.[53] When the cohesive zone size at crack initiation is small compared to the pillar diameter ($l \ll D$), the regime is described as "flaw-sensitive" and the situation is equivalent to an interface crack having a stress singularity at its front. The stress field is characterized by the stress intensity factors, K_I (Mode I crack) and K_{II} (Mode II crack). Note that the detachment is dominated by tension and is therefore almost a Mode I phenomenon. The asymptotic interfacial stresses ahead of the crack are given by

$$\sigma_{22} = \frac{K_I}{\sqrt{2\pi\xi}} \text{ and } \sigma_{12} = \frac{K_{II}}{\sqrt{2\pi\xi}} \tag{5}$$

where ξ is the distance from the crack tip as shown in **Figure 2**a. Based on the analysis of Khaderi et al.,[52] the stress intensity factors are given by

$$K_I = 2.6 H_1 l^{0.094} \text{ and } K_{II} = 0.8 H_1 l^{0.094} \tag{6}$$

where l is the crack length as shown in Figure 2a. At detachment, the strain energy release rate is given as

$$\mathcal{G} = \frac{1-\nu^2}{E}\left(K_I^2 + K_{II}^2\right) = \frac{2.8\sigma_A D^{0.81} l^{0.19} \tilde{a}^2}{E} \tag{7}$$

where E is the elastic modulus and ν is Poisson's ratio, being 0.5 in accordance with incompressibility. In equilibrium and assuming that the detachment is mainly Mode I, the energy release rate equals the thermodynamic work of adhesion, W_{ad}. Hence, the maximum applied stress, $\sigma_{A,max}$, at detachment, which is referred to as the pull-off stress, σ_p, is predicted to be given by

$$\sigma_p = \frac{2.16\sqrt{E \cdot W_{ad}}}{D^{0.406} l^{0.094}} \tag{8}$$

Inspection of Equation (8) provides the scaling of the pull-off stress with the diameter of the flat punch in the flaw sensitive regime: a thinner punch provides better the adhesion in line with our previous experiments with systematically varying pillar diameters (Figure 2b). The power law obtained from the experiment is in accordance with the predicted scaling of –0.406.

For the flaw-sensitive regime ($l \ll D$), Equation (8) further states that the size of initial (short) crack does not significantly affect the resulting pull-off stress, because of $\sigma_p \sim l^{-0.094}$. This is a consequence of the rapidly diminishing stress as the crack advances along the stress singularity. This result is of practical interest, as imperfections at the punch edges cannot be avoided in fabrication,[54] but are predicted to have a minor impact on the adhesion strength. The adhesion strength further scales, as expected from fracture mechanics, with the square root of the elastic modulus, i.e., stiffer punches adhere better to a rigid substrate than softer ones.

It must be noted that there is a limit at which the pull-off stress ceases to be flaw sensitive. When the diameter of the punch approximately equals the extent of the cohesive zone, the cohesive stress dominates. Then detachment occurs as a cohesive failure, i.e., simultaneously at a critical separation distance

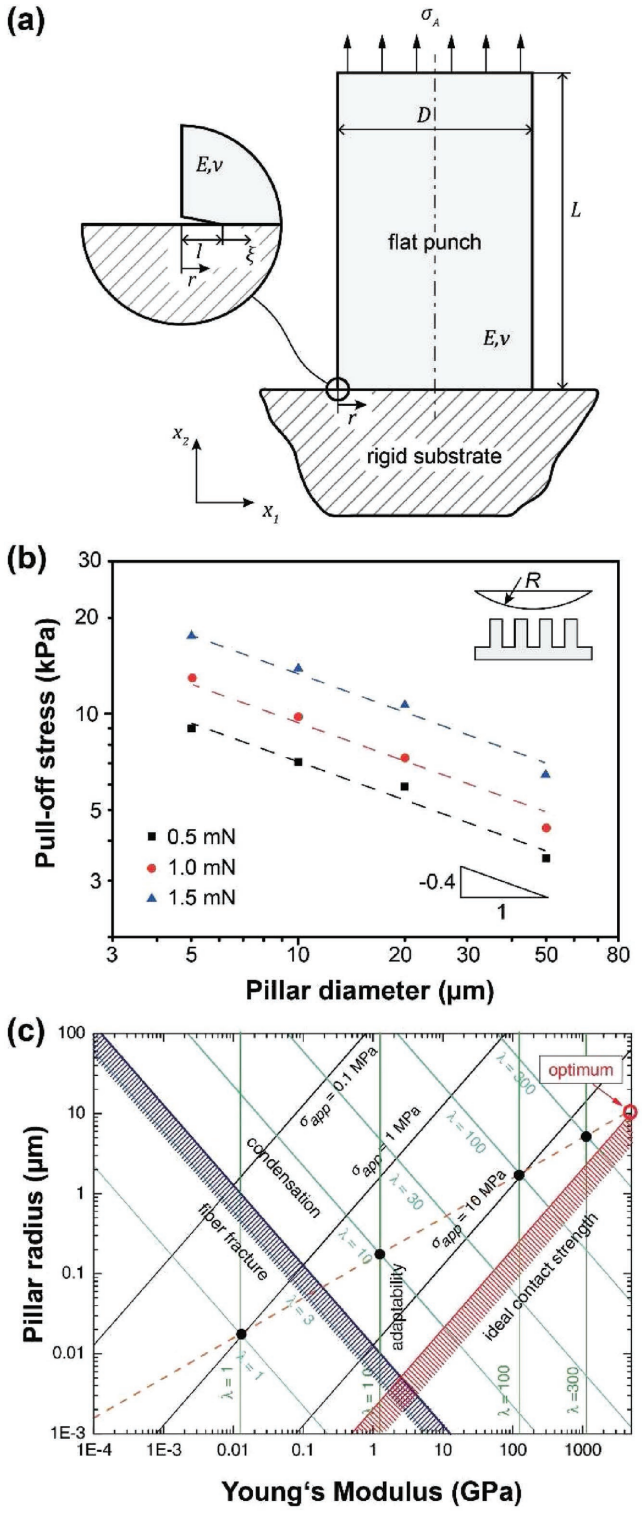

Figure 2. Elastic flat punch adhering to a smooth, rigid substrate. a) A linear-elastic flat punch (cylindrical pillar) is attached to a rigid half-space, with a remote tensile stress, σ_A, applied to the top of the punch. The inset illustrates a short crack ($l \ll D$) embedded within the domain of singularity.[52,53] b) Experimental pull-off stress as a function of pillar diameter reported in ref. [39]. A sapphire sphere with radius, R, of 2.5 mm was used. The preload was varied between 0.5 (black) to 1.5 mN (blue). The dashed lines represent linear fits with a linear slope of −0.4, representing the power law according to Equation (8). c) Adhesion design map for an array of flat punch structures with a packing density of 10%. The blue shaded line indicates the criterion of fiber fracture, the red shaded line the ideal contact strength. The limit of fiber condensation is indicated by the cyan lines and the adaptability by green ones. The black lines are contours of equal apparent contact strength. The dashed line (orange) is the "conode." Its intersection with the ideal contact strength criterion indicates optimum parameters and is highlighted with a red circle. For the calculations, the characteristic length of surface interactions was 0.2 nm, the adhesion energy was 0.05 J m^{-2}, and the effective elastic modulus was 1 MPa. (c) Reproduced with permission.[65] Copyright 2009, Elsevier.

without crack formation and propagation.[41,55] Another limitation is that the analysis is based on complete contact between two perfectly smooth solids. As soon as surface roughness is involved, a tradeoff will appear between surface minimization by contact formation and strain energy build-up induced by deformation of the surface asperities; in such a case, softer punches will perform better than stiffer ones.[56,57]

In addition to the pull-off stress required for detachment, the work necessary to separate two adhering solids is an important parameter to fully characterize the adhesion performance.[41,55,58,59] Splitting of an adhesive contact leads to an extrinsic contribution to the work of separation due to abrupt blunting of a crack when an individual pillar detaches.[41,60] This means that the concentrated stress field is then redistributed over a zone greater than the dimensions of the pillar. For ongoing detachment, a crack must be reinitiated at the next pillar ("crack trapping"). The elastic strain energy, U, stored in a single pillar is

$$U = \frac{\sigma_A^2}{2E} \pi D^2 L \tag{9}$$

where L is the length of the pillar. This energy is dissipated during pull-off. In addition, the free energy required to create a new surface is related to the thermodynamic work of adhesion, W_{ad}. Consequently, the work of separation, W_{sep}, required to debond a punch from a substrate is

$$W_{sep} = \pi D^2 \left(\frac{\sigma_p^2}{2E} L + W_{ad} \right) \tag{10}$$

where σ_p is the pull-off stress. Inspection of Equation (10) indicates that, to significantly enhance the work of separation, the condition $\sigma_p^2 L \gg 2E W_{ad}$ must be met. Therefore, the elastic modulus should be small, the pillars long and their individual pull-off stresses high. This theoretical concept holds also true for more complex geometries such as film-terminated pillar arrays[61,62] or subsurface microchannels.[63] In such specimens, the effective modulus can be tuned by structural features and, thereby, crack trapping and the compliance of the adhesive contact can be controlled.

For the rational design of micropatterned adhesives, Spolenak et al.[64] and Greiner et al.[65] proposed design maps that predict the optimal pillar geometry as functions of their elastic properties and structural parameters (Figure 2c). The maps include limits such as cohesive strength, agglomeration or clustering of pillars, and an upper limit for the pull-off strength. Maps for different contact geometries can be quite complex and

may, for this reason, not have received the attention they deserve for the optimization of micropatterned adhesives.

The contact splitting principle exhibits further practically important aspects. For example, the effective contact stiffness of a micropatterned adhesive is smaller compared to unpatterned, monolithic adhesives. This larger compliance of the contact can lead to an enhanced contact area to rough surfaces or curved objects accompanied with a reduced strain energy penalty.[66–68] Moreover, high aspect ratio pillars tend to be mechanically uncoupled, which means that elastic distortions of an individual pillar (e.g., due to an asperity) do not affect adjacent pillars. However, the adhesion of micropatterned adhesives to rough substrates is subject to certain limitations such as pillar condensation or clumping,[65,69] which can in principle be avoided by the implementation of hierarchical levels.[68,70]

A practical aspect limiting the reliability and longevity of micropatterned adhesives is the deterioration of adhesion in the presence of dirt or dust. A self-cleaning capability would be advantageous but requires that the fibrils are made from non-tacky materials. For contaminated gecko toe pads consisting of β-keratin, Hansen and Autumn demonstrated recovery of the adhesion strength upon a few steps on a clean substrate.[71] The effect relies on the higher adhesion of the dirt particles on the substrate compared to the adhesion on the individual fibrils. Clemente et al. performed similar studies with insects and compared the self-cleaning capability of fibrillar and smooth adhesives pads.[72] Hairy pads were found to recover two to ten times faster than smooth pads. It was further argued that self-cleaning is supported by shear movements to wipe off contaminations.[72,73] In this context, a saving grace of micropatterned adhesives is their higher defect tolerance: partial pollution or damage of individual fibers does not necessarily impact the overall performance because crack trapping mechanisms are still in place in the intact areas.[42,74] This is in contrast to unpatterned adhesives, where local defects of a critical size can grow throughout the contact area without arresting.

2.2. Design of Contact Geometry: Mushroom and Funnel-Shaped Tips

The previous section demonstrates that the interfacial mechanics is at least as important as surface chemistry for understanding adhesion of micropatterns. This explains why, as has been realized early on in the observation of natural adhesive surfaces,[6,75] the details of the contact geometry play a key role in optimizing adhesion performance. The dock beetle, for example, exhibits fibrils on its adhesive pad with tip geometries ranging from conical, spatula-shaped to mushroom-shaped (**Figure 3**). Bullock and Federle found that the adhesion strongly differs for each type of fibril: The highest pull-off forces were obtained for mushroom-shaped tips, characterized by a gradual widening toward the tip face.[45]

Even without a full understanding of the mechanisms involved, mushroom-shaped tips have subsequently been used as a blueprint for many synthetic structures.[76–78] In several experiments, it was demonstrated that a mushroom-shaped pillar can enhance the pull-off stress by up to one order of magnitude over flat punch pillars.[40,79–82] Because of the re-entrant geometry, such structures are however not straight forward to fabricate. One possibility is to modify the tips of previously manufactured (straight) pillar structures by a dipping process:[78,83–85] droplets of a liquid prepolymer are squeezed between the pillar face and a substrate to form a meniscus on each pillar. The prepolymer is then cross-linked to form a stable contact region. The process works for most materials with nonvolatile prepolymers, such as polydimethylsiloxanes or polyurethanes. The formation and final geometry of the mushroom tip depends mainly on the wettability of the substrate and the pillar surface, the volume of the droplet, and the shrinkage during cross-linking. As an alternative approach, master structures representing a negative of the complete structure of the mushroom pillar can be used for replication (see, e.g., **Figure 4**c).

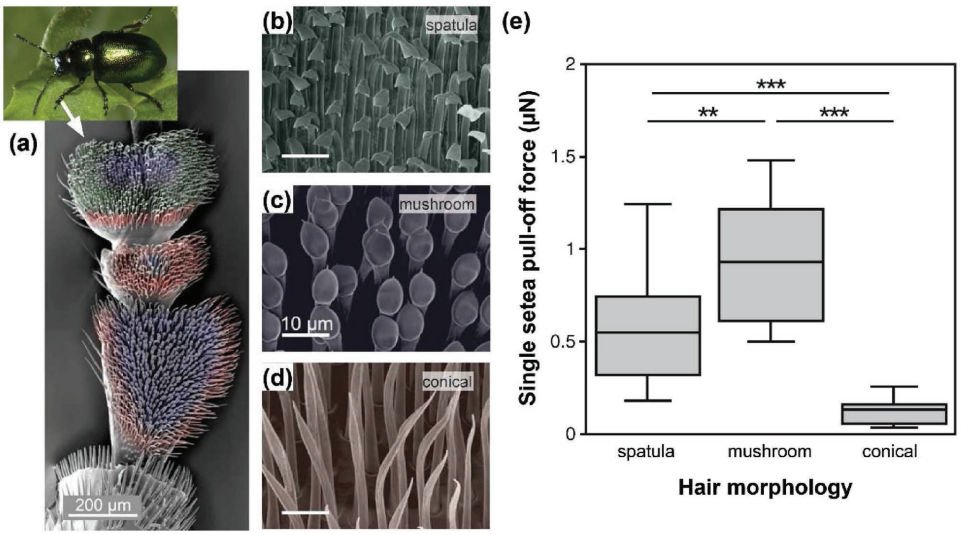

Figure 3. Adhesive pad morphology of male dock beetle G. viridula. a) Scanning electron image of three tarsal pads of the hind leg consisting of different fibril shapes. b–d) Adhesive fibrillar hairs with different terminal contact elements: b) spatula, c) mushroom, d) conical. e) In vivo single hair measurements. Pull-off forces for the three seta types. The plot shows medians (center lines), interquartile ranges (boxes), and the largest and smallest values (whiskers). All panels reproduced with permission.[45] Copyright 2011, Springer.

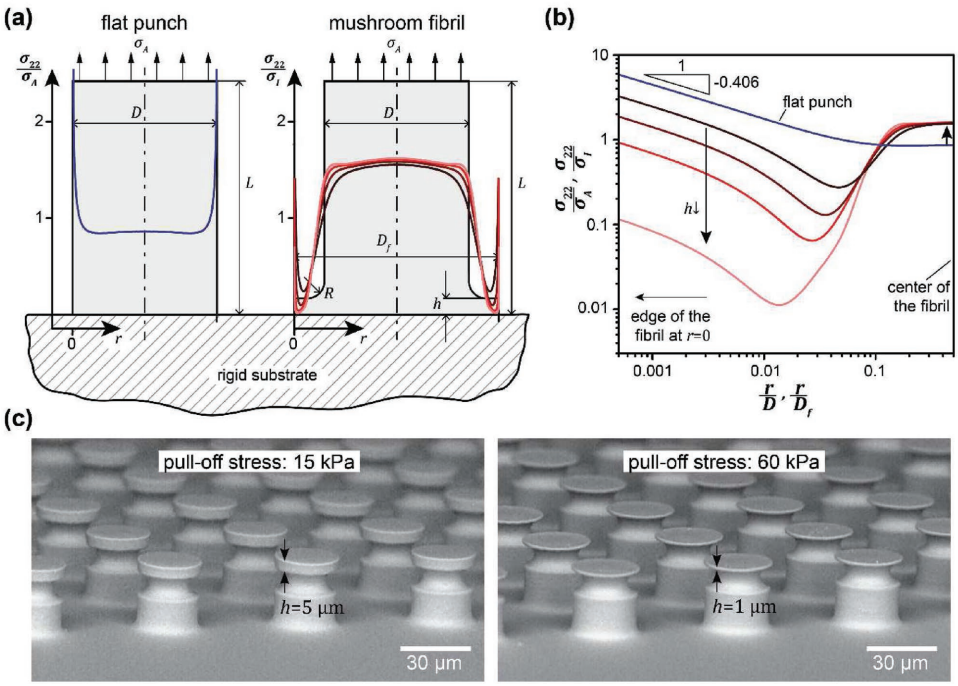

Figure 4. Flat punch versus mushroom structures in analysis and experiment. a) A linear-elastic flat punch (left) and mushroom structure (right) attached to a rigid half-space, with a remote tensile stress, σ_A. The lines show the normalized tensile stresses σ_{22}/σ_A and σ_{22}/σ_I, where σ_I is the average stress along the structure–substrate interface for varying flap thickness, h. (a,b) Reproduced with permission.[87] Copyright 2016, Elsevier. Note the shift from detrimental singular edge stresses in the flat punch to lower edge stresses at the edge of the mushroom flaps. b) Normalized tensile stress σ_{22}/σ_A and σ_{22}/σ_I along the structure–substrate interface from (a) plotted in log–log scale. The slope of –0.406 represents the asymptotic solution of the edge singularity for an elastic flat punch adhering to a rigid substrate, see also Equation (8).[52] The magnitude of the singularity decreases with decreasing h, whereas the center stress increases (trends highlighted by arrows). Reproduced with permission.[87] Copyright 2016, Elsevier. c) Scanning electron images of mushroom structure arrays generated via two-photon lithography and subsequent molding into polydimethylsiloxane. Pull-off stresses follow the trend predicted by the simulation. The values were calculated by dividing the pull-off force by the apparent contact area.

The mechanistic understanding of the improved adhesion of mushroom-shaped fibrils has been a focus of research attention in recent years. A significant discovery is related to the distribution of normal stresses inside the contact area. Flat punches in adhesive contact with a rigid substrate invariably exhibit stress singularities at their edges, at least for experimentally relevant conditions of finite interfacial friction and differing Poisson ratios (Figure 4).[86] For fibrils with mushroom shape, it is generally found that the magnitude of the edge singularity is greatly reduced, whereas the stresses at the center of the contact simultaneously increase.[86–89] The actual stress distribution (Figure 4a,b), however, varies strongly with the geometry of the tip. As a result of the simulations, low edge stresses are favored in wide but thin mushroom flaps (large D_f and small h in Figure 4a).

Some of these theoretical predictions have been verified experimentally, at least in a qualitative sense. A recently established method that allows high spatial control in the generation of micropatterned surfaces is two-photon lithography, which enables 3D patterning with a resolution down to 300 nm.[90] Using this method, we fabricated mushroom-shaped pillars with 1 and 5 µm thick flaps, while keeping all other dimensions constant (Figure 4c). The structures with the thinner flaps exhibited pull-off stress that were higher, by a factor of 4, than the thicker flaps.[87] However, there exists a practical limit beyond which very thin and wide mushroom flaps become mechanically unstable.

An alternate design introduced recently are funnel-shaped microstructures (**Figure 5**).[91] Here, the flaps are conically arranged, which improves their mechanical stability (Figure 5a). These structures were again generated by two-photon lithography. In adhesion tests on single features, a characteristic behavior was identified: Upon initial contact, the flexible flaps deform readily as is expressed in a shallow slope of the compressive loading curve (Figure 5b). At this stage, the bending of the flaps efficiently accommodates surface irregularities and even small misalignments between structure and substrate. The next stage is axial compression of whole structure, which is reflected in a higher elastic slope. After stress reversal, exceptionally high adhesion values of up to 5.6 MPa (with respect to the real contact area) were measured for single structures. This value is at least an order higher than previously reported results for van der Waals-based reversible adhesion. It was found to be hardly affected by ambient air pressure, which rules out suction as an essential contributor to adhesion. We hypothesize that the outstanding performance is due to an increased real contact as a result of the large-scale deformation and that the interfacial stress distribution is more conducive to adhesion in these structures; however, a satisfactory

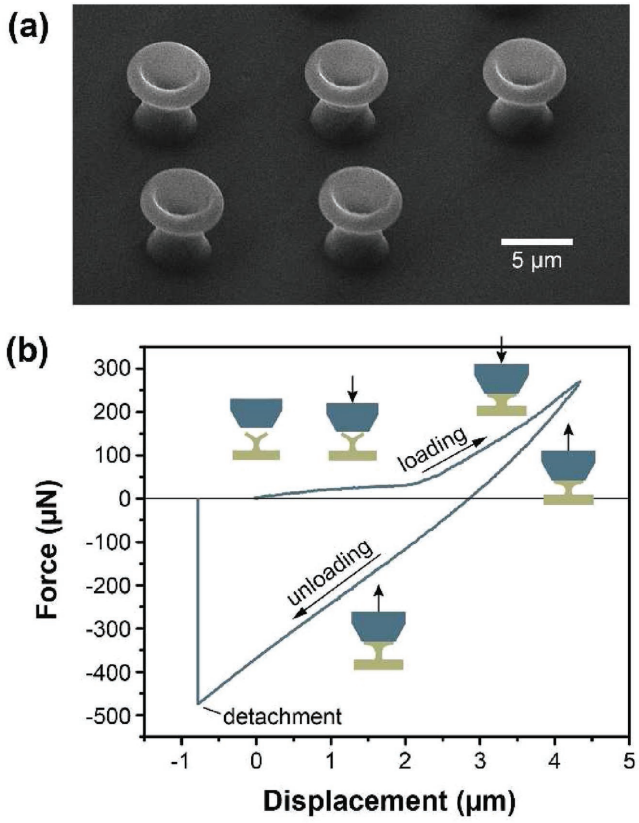

Figure 5. Funnel-shaped microstructures proposed as a new design. a) Scanning electron image of funnel-shaped microstructures fabricated using two-photon lithography and subsequent replication into poly(ethylene glycol) dimethacrylate. b) Typical force–displacement curve: The compressive loading curve (positive force) comprises two parts with different slopes corresponding to bending of the flaps transitioning into compression of the whole structure. The unloading curve (negative force values) terminates at a maximal tensile force, indicating pull-off. Adhesion is exceptionally high and surpasses all published data. Reproduced with permission.[91] Copyright 2017, Wiley-VCH.

theoretical picture is not yet available. Another current limitation is that it remains yet to be seen how these structures perform as large arrays.

2.3. Composite Structures

In addition to contact geometry, the material properties of a pillar structure can be modified to modulate adhesion. The ladybug, as an example from nature, exhibits adhesive fibrils with an axial gradient of the elastic modulus. From the stalk to the tip, the elastic modulus decreases by three orders of magnitude, from 7 GPa to ≈1 MPa.[92] Similarly, the smooth adhesive pads of stick insects exhibit an elastic gradient, terminating in 200 nm thick and ≈10 kPa soft epicuticular layers.[93] Making contacts softer while keeping stalks stiff has two major advantages: First, the tips adhere better to rough surfaces due to reduced elastic strain energy expended. And second, stiff stalks maintain the mechanical stability of the microstructure avoiding agglomeration and clustering. Gorb and Filippov further demonstrated that this holds true even for high aspect ratio pillars adhering to rough substrates.[69]

First synthetic adhesives with such a "composite" structure were reported by Murphy et al.[94] They fabricated tilted pillar structures and added soft mushroom tips via dipping as described in Section 2.2. It was demonstrated that softer tips could improve both the adhesion and the friction performance. Using a similar approach, Bae et al. added softer tips to a prepatterned array and demonstrated improved adhesion to skin.[36] Minsky and Turner performed experiments and simulations using composite posts with a stiff core and a soft shell.[95,96] Very thin soft tip layers were again found to promise the best adhesion enhancements for smooth substrates.

Balijepalli et al. theoretically investigated the interfacial stress distribution of composite pillars with stiff stalks terminated by soft tip layers.[97] The design parameters investigated were the thickness of the soft tip layer, the ratio of the elastic moduli, and the curvature of the interface between the two materials (**Figure 6**). The pull-off strength values were predicted to increase for thinner layers and larger modulus ratios in accordance with experimental results on model structures (Figure 6a).[98] For all elastic modulus ratios, a thinner layer resulted in a decreased magnitude of the edge stress singularity, whereas the stress at the center was increased related to a "confinement" effect.[99,100] Furthermore, the increment of the energy release rate during detachment varied with the extent of confinement. This means that with decreasing film thickness (i.e., larger degree of confinement), the detachment mechanism changes from unstable growth of edge cracks to more stable growth of finger-like or center cracks.[98–100] It should be noted that the effect due to confinement of the soft terminal layer depends strongly on material compressibility (i.e., Poisson's ratio).[99] The curvature of the interface was found to strongly affect the tensile stress distribution along the pillar-substrate interface, particularly for very thin films. The simulations indicate that higher curvatures lead to enhanced tensile stresses at the center; this is in harmony with the experiments, in which a transition from edge to center crack detachment was observed.[98] In addition, composite structures exhibited similar adhesion in the presence of finite substrate roughness, whereas adhesion dropped by more than 50% for a flat punch pillar (Figure 6c). As almost all objects exhibit surface roughness on a scale relevant for van der Waals interactions, this concept may be an important step toward practical applicability of micropatterned dry adhesives.

2.4. Directional Adhesives

Micropatterned adhesives that adhere or detach in a preferred direction in the plane of the surface, are often referred to as directional adhesives (**Figure 7**). This topic has been extensively reviewed by others so we will only highlight some fundamental working principles.[17,101–104] In nature, directionality allows for fast locomotion. Most animals having fibrillar adhesives utilize enhanced shear adhesion or frictional adhesion by pulling their adhesive pads toward their body; to detach by, the fibrils are pushed away from the body to initiate peeling (Figure 7a). The adhesive pads consist of fibrils tilted

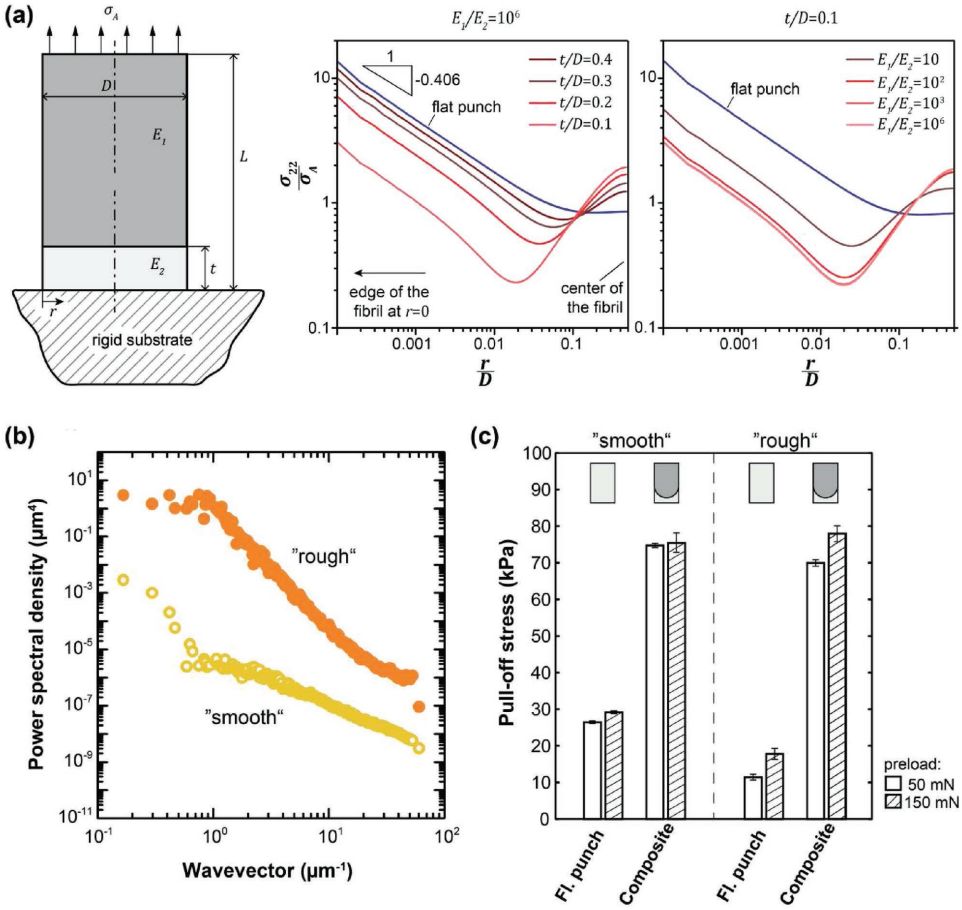

Figure 6. Composite structures in analysis and experiment. a) A composite structure with $E_2 < E_1$ adhered to a rigid half-space. For a remote tensile stress, σ_A, the normalized tensile stress distribution, σ_{22}/σ_A, is shown for different confinement ratios, t/D, at constant elastic modulus ratio, $E_1/E_2 = 10^6$ (left) and for different elastic modulus ratios, E_1/E_2, at constant confinement of the soft terminal layer, $t/D = 0.1$ (right). Reproduced with permission.[97] Copyright 2017, Elsevier. b) Power spectral density in terms of the wave vector for two glass substrates designated as "smooth" and "rough". Reproduced with permission.[155] Copyright 2017, IOP. c) Pull-off stress as a function of surface roughness and pillar design. The values were calculated by dividing the pull-off force by the real contact area of a single pillar. Composite pillars with hemispherical interface soft/stiff show higher adhesion and lower sensitivity to roughness than flat punch pillars. Tests performed at different preloads: 50 mN (white bars) and 150 mN (hatched bars). Reproduced with permission.[98] Copyright 2017, the Authors. Published by ACS.

in a direction opposite to the pulling direction (Figure 7b,c). Experiments have demonstrated that the friction of a pillar array with tilted pillar structures strongly depends on the loading direction and the tilt angle of the fibers. The friction in direction of tilted fibers can be up to 100% higher than against the tilt direction.[19,94,105–108]

Moreover, directionality of micropatterned adhesives without any predefined tilt of the structures can be introduced by non-symmetric pillar designs, in order to control the contact area in a friction experiment for instance (Figure 7d,e).[108–110] Modification of the tip shape provides another playground for directionality without the need of tilted structures. Inspired by the gecko, spatula shaped tip geometries have been put forward as a promising concept for directional synthetic micropatterned adhesives.[40,111,112] Sameoto and Menon introduced a method to precisely control the offset between the pillar and the spatula tip and found that the amount of cap size overhang controls the peel strength.[113] Another concept for directional adhesives is the implementation of defects at the tip faces that act as starter cracks and, therefore, initiate the delamination during pulling.[114,115]

3. Applications

3.1. Climbing and Crawling Robots

The substantial knowledge and understanding obtained over the last decade have enabled the initial transfer of the biological inspiration into specific applications (**Figure 8**). An exciting field is the design of crawling and climbing robots equipped with micropatterned adhesives for locomotion in terrestrial and extraterrestrial use (Figure 8d).[32,116,117] ABIGAILLE is a robot developed by Menrva lab of Simon Fraser University, where six legs equipped with mushroom-shaped dry adhesives can adhere to a vertical surface and detach via a peeling motion to climb a surface.[25,118,119] The Cutkosky lab at Stanford University has developed robots a few centimeters in size based on

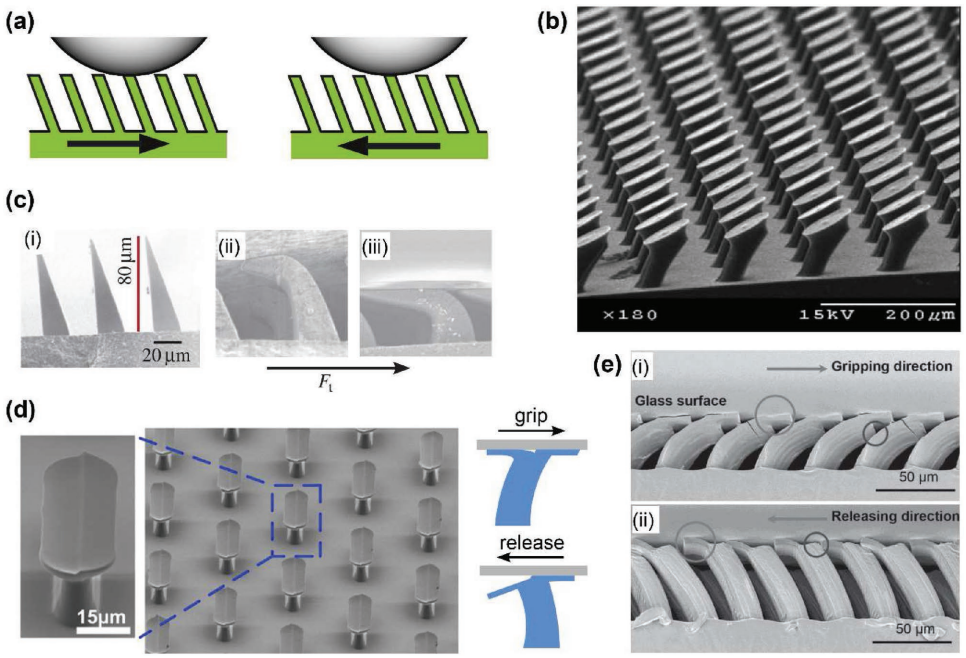

Figure 7. Directional adhesives. a) Typical setup for testing anisotropic frictional adhesion induced by tilted pillars. Reproduced with permission.[94] Copyright 2007, Taylor & Francis. b) Electron image of tilted fibrils with angled mushroom tips. Reproduced with permission.[105] Copyright 2009, Wiley. c) The contact area and, therefore, adhesion of microwedges are enhanced on applying shear load, F_t. Reproduced with permission.[169] Copyright 2015. The Royal Society Publishing. d,e) Electron images of straight micropillars with steps at the tip faces for directed gripping and releasing. (d) Reproduced with permission.[115] Copyright 2016, ACS. (e) Reproduced with permission.[108] Copyright 2014, Wiley.

directional shear adhesives, called microTugs.[27,28] These robots stick to the surface while pulling a multiple of their own weight. In the same lab, the StickyBot has been developed.[26,29] Its four legs, mimicking the hierarchical assembly of the gecko foot, are optimized for shear adhesion to vertical walls. The StickyBot can climb smooth surfaces at a speed of several cm/s and could be potentially used for inspection, maintenance, surveillance or disaster relief.

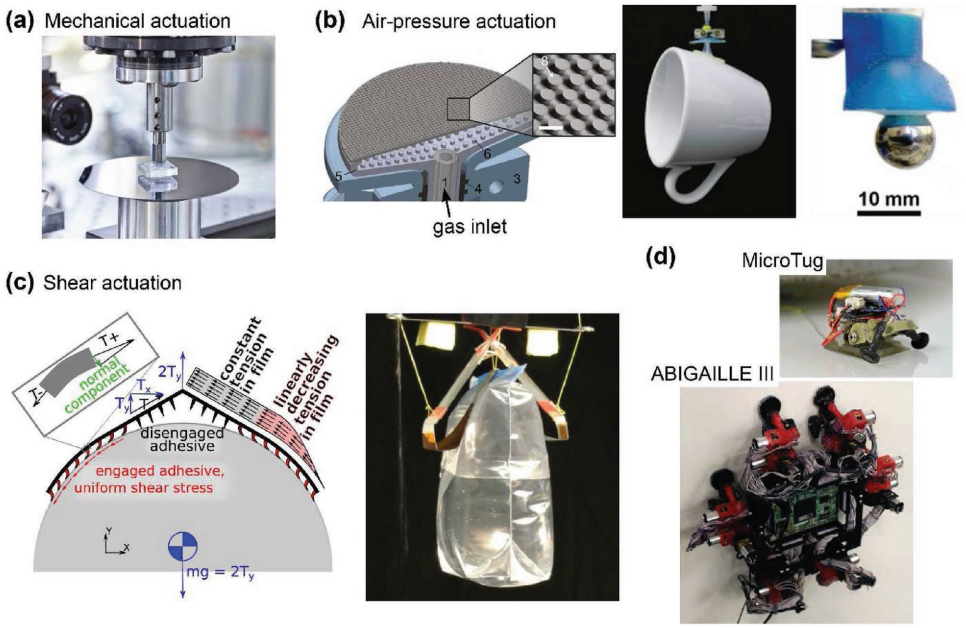

Figure 8. Some applications of micropatterned dry adhesives. a) Reversible pick-and-place handling of fragile silicon wafers using mechanical actuation (for details, see Figure 9). b) Pick-and place of curved objects using air-pressure actuated systems. Reproduced with permission.[24] Copyright 2017, National Academy of Sciences and rightmost panel reproduced with permission.[123] Copyright 2014, Wiley. c) Gripper equipped with directional adhesive (see Figure 7c) for frictional adhesion. Reproduced with permission.[122] Copyright 2015, IEEE. d) Examples for climbing and crawling robots equipped with micropatterned adhesives: ABIGAILLE climbs smooth vertical walls; microTugs pulls payloads much larger than its own mass. Reproduced with permission.[119] Copyright 2014, Elsevier and Reproduced with permission.[27] Copyright 2015, IEEE.

3.2. Pick-and-Place Handling

Another field of application is the handling of objects and components in production lines. Pick-and-place devices typically rely on temporary adhesion based on mechanical gripping, suction, electric, or electromagnetic devices. The recent progress in research and development of micropatterned adhesives reveals that such a technology could be an alternative to the existing ones. Pick-and-place of objects was demonstrated by several groups: Examples range from handling of fragile objects such as silicon wafers or thin glass sheets,[22,23,120] micro-objects such as silicon platelets,[96,121] to 3D objects such as curved objects or bags (Figure 8a–c).[24,122,123]

In our group, a six-axis robot equipped with micropatterned adhesives has demonstrated the handling of fragile objects such as wafers, screen glasses, lenses, and paper (**Figure 9**a). Such a handling platform is highly energy-efficient, as the actuation does not require external energy, and works virtually silently. It may revolutionize advanced handling solutions, where suction devices and mechanical grippers are beginning to face insurmountable limits.

To reliably grip and release objects, the key is the switchability between an adhesive and a nonadhesive state. An elegant mechanical approach is to control the compressive load applied to the adhesive structures: In the attachment phase, a small preload is sufficient to create contact and adhesion to the object; to initiate release, a compressive overload induces an elastic instability due to buckling of the pillars and creates a nonadhesive state (Figure 9b,c).[20,124–127] Such a load-controlled stimulus represents a reliable strategy and is easy to implement into industrial robotic systems. Building on this concept, Yagüe and Kroner developed multistep switchable adhesives.[128] Here, pillar structures of various lengths allowed for tuning of the pull-off force. At low preload, only long pillars formed contacts with the object, resulting in a low pull-off force; at higher preload, all pillars were brought in contact, giving a high pull-off force. Additional further loading again induced buckling and release. Different strategies are feasible to control the adhesion performance by varying the actual contact area. Established concepts to bend pillars are temperature variation in combination with trained shape memory polymers[129,130] or shape memory alloys as a backing layer.[131] In addition, magnetic fields or UV light can trigger the bending of pillars with incorporated magnetic or light sensitive components.[132–135]

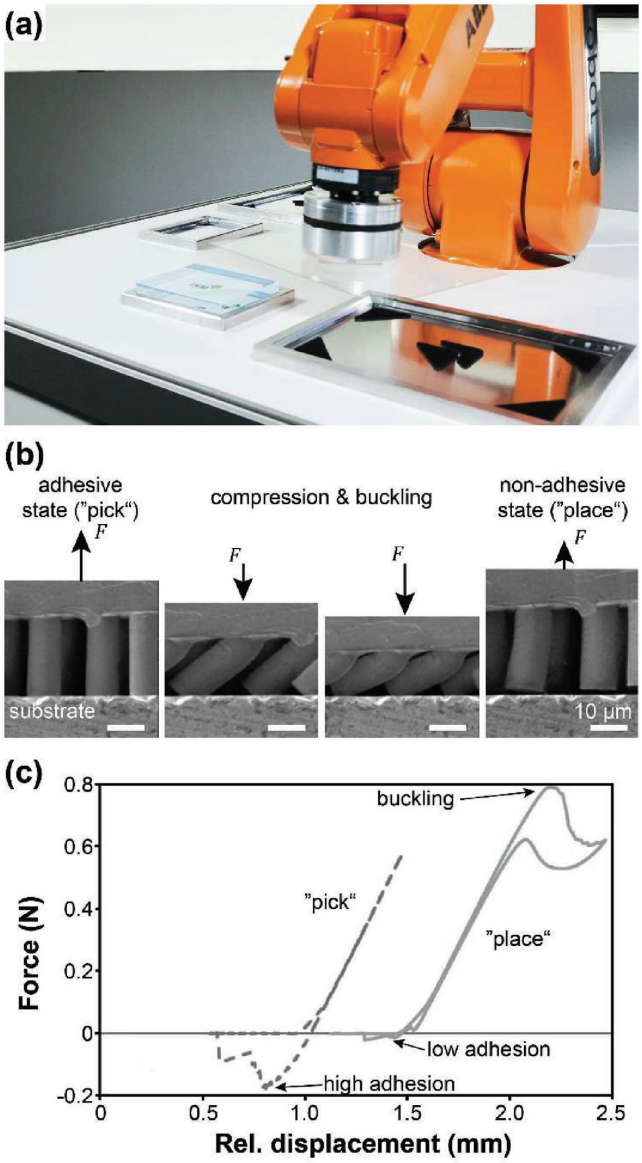

Figure 9. Demonstration of switchable adhesion for pick-and-place handling. a) Six-axis robot equipped with micropatterned dry adhesive demonstrating handling of fragile screen glasses. b) Switching of the adhesion strength by fiber reorientation. Side-view observations of micropillars in a scanning electron microscope simulating a pick-and-place cycle. Sequence starts with contact formation leading to an adhesive state ("pick," left). Compressive overload results in bending and buckling of micropillars, facilitating detachment (center). Release of the substrate in a nonadhesive state ("place," right). Reproduced with permission.[20] Copyright 2011, Elsevier. c) Force–displacement curves for "pick" and "place." The hysteresis in the compressive preload is related to the nonlinear buckling of the microstructures. Reproduced with permission.[128] Coypright 2015, Wiley-VCH.

3.3. Long-Term Performance

Pick-and-place involves the repeated contact and deformation of the micropatterned features, raising questions about the durability of the microstructures. Only few long-term tests are available that provide information on the resistance against cyclic loading, the material degradation and the contamination of structures with increasing number of contact events. The results of such a long-term test are displayed in **Figure 10**. An adhesive structure (here made from Sylgard 184, Dow Corning, USA) repeatedly picked up and released a metal plate. Following predefined numbers of cycles, the pull-off stress was repeatedly measured (Figure 10a). We found that the micropatterned adhesive could go through numerous pick-and-place cycles before a degradation of its adhesive performance was noticeable. In this particular case, a decrease of pull-off stress was observed after about 10 000 cycles. Subsequent scanning electron microscopy revealed that this was related to a degradation of the material, particularly due to cracks that appeared

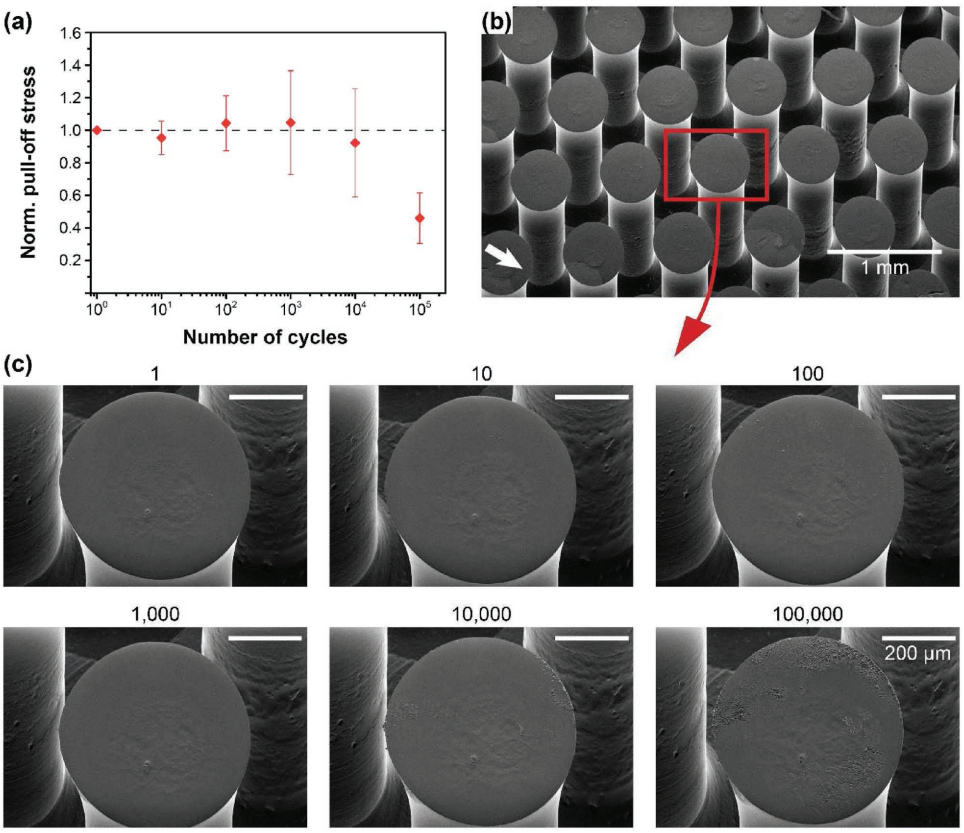

Figure 10. Long-term simulation of pick-and-place cycles. a) Pull-off stress as a function of the number of attachment–detachment cycles. The stresses were normalized by the pull-off stress obtained in the first cycle. Error bars represent the standard deviation determined from three tests. b,c) Scanning electron images of the micropatterned adhesives related to the adhesion measurements. c) Insets show the morphological variation of an individual pillar face with increasing number of cycles.

in the contact area (Figure 10b,c). In addition, residues of free oligomers or silicone oils were detected on the substrate. This result was not unexpected, as Sylgard 184 is known to contain these components.[136] The durability of micropatterned adhesives will depend on the loading conditions and the details of the handling process; under other circumstances, reliable handling up to more than 500 000 cycles was recorded. Further work needs to be done to identify the governing degradation mechanisms and to identify appropriate counter measures.

In general, the long-term performance will be strongly related to the material selection. Material properties determine the durability against mechanical degradation such as wear and fatigue. Material formulations should be carefully chosen to avoid volatile compounds, fillers, and liquids not bound to the network, and other easy to release components. Stiffer materials are less sensitive to contamination by particles and dust because they are usually less sticky and therefore easier to clean.[137] A balance between this sensitivity and the adhesive performance will have to be found to optimize these structures.

4. Operating Conditions

Over the last two decades, synthetic micropatterned adhesives have nearly exclusively been optimized for smooth surfaces and have been mostly tested under controlled conditions such as room temperature and constant relative humidity. However, these conditions may strongly vary for potential applications in a real production environment.

4.1. Surface Roughness

Surface roughness is a well-known opponent of adhesion. Roughness is therefore an essential determinant limiting adhesion of current micropatterned adhesives and, hence, the maximum lifting force.[70,138–144] An increase in roughness leads to larger distances over which the van der Waals interactions have to act because the adhesive does not completely conform to the surface topography.[145] As a consequence, the contact area at which the interactions contribute to adhesion is much smaller than the apparent area.[146–148] In addition, the adhesive stores higher elastic strain energies at the contact zone, which also counteracts adhesion.[56,149–152] To improve adhesion, higher preload and, in case of viscoelastic materials, longer contact times can help to enlarge the adhesive contact area.[153,154]

The size of surface features on a rough surface often varies from atomic to micron or even millimeter scale; hence roughness can only be described by statistical parameters. In a recent review, Jacobs et al. discuss the importance of the power

spectral density (PSD) as an accurate mathematical tool to quantitatively describe the surface topography (see Figure 6b).[155] A PSD contains all statistical information on spatial frequencies in the signal unaffected by the characterization method. Several contact mechanics models exist for computing the adhesive properties of rough interfaces. All of them can use the PSD as an input, regardless of whether the entire PSD is used as in Persson's theory[156,157] or whether scalar quantities calculated from the PSD such as the root-mean-square (RMS) height, the RMS slope or the RMS curvature are employed.[147,148,158,159] In any case, the measurement and calculation of accurate, reliable PSDs of real-world surfaces is most important for practical applications.[155]

In contrast to unpatterned adhesives, micropatterned or fibrillar adhesives exhibit features with lateral (horizontal) dimensions. Therefore, RMS or the mean peak-to-valley profile roughness is not sufficient to characterize adhesion; RMS slope or mean distance parameters should be considered instead. In a recent study by Barreau et al., the pillar diameter and the height of micropatterned adhesives were varied systematically (**Figure 11**a).[68] From this, a first strategy for dealing with surface roughness has emerged: For the best adhesion performance, the pillar diameter should be small to take advantage of the contact splitting effect as discussed in Section 2.1. However, the pillar diameter D should not be smaller than the mean spacing between local peaks, S, on the substrate. When $D > S$, the structures undergo only small elastic deformations during contact formation. By contrast, when $D < S$, bending and buckling events cannot be avoided, which store more energy, reduce the contact area, therefore, lead to nonadhesive characteristics (Figure 11b). To obtain the highest compliance, the pillars should be as long as possible without jeopardizing stability of the structures.

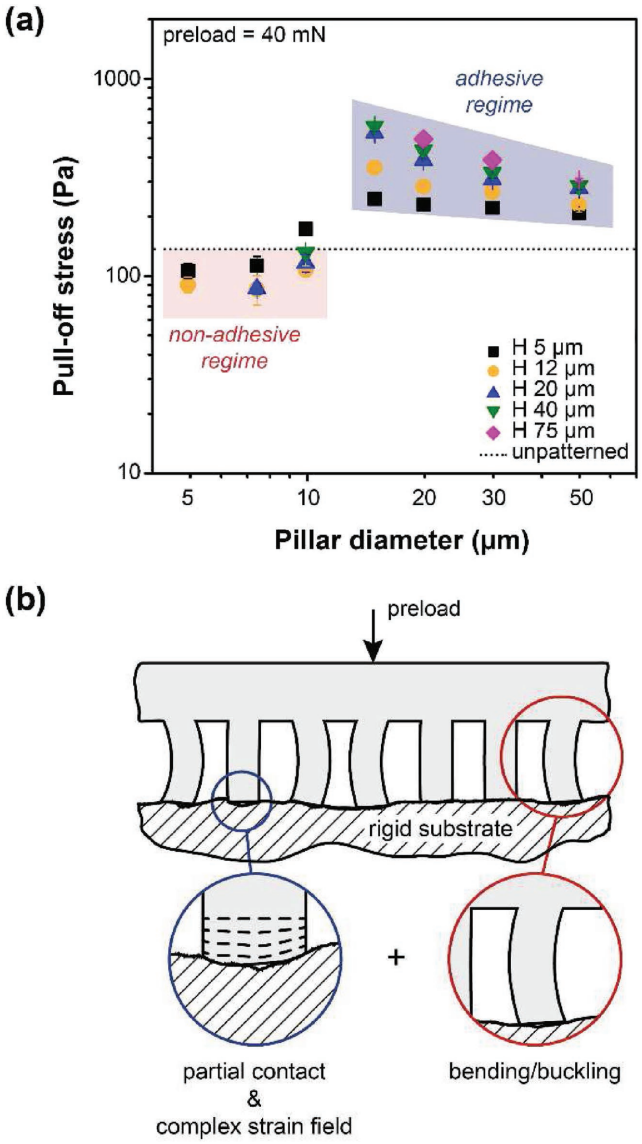

Figure 11. Adhesion of micropatterned adhesives to rough substrates. a) "Adhesive" and "nonadhesive" regimes for polydimethylsiloxane (PDMS) pillar arrays on a rough glass substrate (mean peak-to-valley distance, R_z = 5.8 μm, and a mean spacing between adjacent peaks, S = 12.8 μm). The plot represents the effect of pillar diameter and length H on pull-off stress. Dotted line: Pull-off stress of an unpatterned sample. The pull-off stresses were calculated by dividing the pull-off force by the apparent contact area. (b) Hypothetical contact mechanisms in the adhesive and nonadhesive regimes: Schematic of a micropatterned array pressed onto a rough substrate. Insets represent the partial contact and a complex strain field at the pillar faces found to occur in both regimes (inset left). Additionally, bending and buckling of pillars can occur in the nonadhesive regime (inset right). Reproduced with permission.[68] Copyright 2016, Wiley-VCH.

4.2. Temperature

Another critical issue in developing useful adhesives is the elevated operating temperature in many industrial applications. The challenge lies in the fact that mechanical properties of polymers can vary drastically with temperature. Elastomers, which are mainly used for making micropatterned adhesives, exhibit strong temperature dependencies when passing the glass transition temperature, T_g. At T_g, the molecular mobility changes from a glassy state ($T < T_g$) to a flexible rubber state ($T > T_g$), accompanied by a strong decrease of the elastic modulus. Even within the glassy and the rubber states, the mechanical properties may not be constant and, particularly in copolymers, more than one glass transition temperature can be present. Consequently, the elastic modulus is a complex function of temperature, which alters the pull-off stress and the work of separation (see Equations (8) and (10)). For viscoelastic materials, the viscoelastic loss factor exhibits a maximum at T_g. Hence, large amounts of energy are dissipated at T_g as was demonstrated by Zosel for pressure sensitive adhesives.[160–162] However, the adhesion performance is not a simple function of temperature in general: for an ideal contact situation, the higher modulus below T_g can enhance the pull-off stress (see Equation (8)) while preventing intimate contact formation, particularly on a rough surface. Conversely, contact formation may be improved above T_g but the lower modulus can at the same time reduce the adhesion.[163–165] Recently, Barreau et al. demonstrated that adhesion is enhanced by the combination of viscoelasticity and surface micropatterning.[166] In accordance with earlier reports, the glass transition temperature was

identified as the temperature of highest work of separation. In summary, the operating temperature will strongly affect material selection and technical design of polymeric micropatterned adhesive devices.

5. Summary and Perspectives

Dry adhesion of micropatterned polymeric surfaces has reached a mature state of understanding over the last decade. Adhesion performance is primarily controlled by mechanical aspects rather than merely by surface energy and chemistry. As a consequence, the design of the contact geometry and the material properties are key to the creation of high-performance micropatterned adhesives. Based on a contact mechanics approach, the fundamentals of the contact splitting principle and an analysis of the scaling law in adhesion were presented. Optimization of the adhesion behavior requires the avoidance of excessive stress concentrations in the interface, for which two strategies were described: 1) mushroom-shaped structures, as developed by several groups over the last decade, represent a proven strategy to improve the adhesion strength; and 2) composite and 3) funnel-shaped microstructures are more recent concepts offering similar benefits for adhesion. The introduction of asymmetric features can provide a directionality of adhesive properties with a favorable detachment direction for easy release, which is a unique feature of micropatterned adhesives compared to unpatterned adhesives.

Micropatterned adhesives offer novel solutions for rough substrates and under changing temperature conditions. The concept thus offers great potential for engineering a new generation of handling devices. The rising demand for such a new technology brings with it several open questions related to specific applications, such as reliability and long-term durability. The feasibility of large-scale fabrication has recently been demonstrated by roll-to-roll fabrication in the groups of Kwak and co-workers and Jeong and co-workers.[167,168] In this way, the universal phenomenon of adhesion will, through modulation by micropatterning, very likely be exploited in numerous future applications.

Acknowledgements

The authors thank Stefanie Faust for her invaluable help with the TPP-fabrication presented in Figure 4c, and Fabian Altmeyer and Verena Tinnemann for their investigation of the long-term tests presented in Figure 10. The authors acknowledge funding from the European Research Council under the European Union's Seventh Framework Program (FP/2007-2013)/ERC Advanced Grant No. 340929.

Conflict of Interest

The authors declare no conflict of interest.

Keywords

adhesion, bioinspired materials, contact splitting, handling, robotics

Received: February 2, 2018
Revised: March 7, 2018
Published online: April 26, 2018

[1] K. Autumn, Y. A. Liang, S. T. Hsieh, W. Zesch, W. P. Chan, T. W. Kenny, R. Fearing, R. J. Full, *Nature* **2000**, *405*, 681.
[2] E. Arzt, S. Gorb, R. Spolenak, *Proc. Natl. Acad. Sci. USA* **2003**, *100*, 10603.
[3] B. N. J. Persson, *MRS Bull.* **2007**, *32*, 486.
[4] S. N. Gorb, *Functional Surfaces in Biology*, Vol. *2*, Springer, Berlin **2009**;
[5] D. Labonte, C. J. Clemente, A. Dittrich, C.-Y. Kuo, A. J. Crosby, D. J. Irschick, W. Federle, *Proc. Natl. Acad. Sci. USA* **2016**, *113*, 1297.
[6] S. Gorb, R. Beutel, *Naturwissenschaften* **2001**, *88*, 530.
[7] F. Haas, S. Gorb, *Arthropod Struct. Dev.* **2004**, *33*, 45.
[8] W. Federle, *J. Exp. Biol.* **2006**, *209*, 2611.
[9] N. E. Stork, *J. Nat. Hist.* **1983**, *17*, 583.
[10] K. Autumn, M. Sitti, Y. A. Liang, A. M. Peattie, W. R. Hansen, S. Sponberg, T. W. Kenny, R. Fearing, J. N. Israelachvili, R. J. Full, *Proc. Natl. Acad. Sci. USA* **2002**, *99*, 12252.
[11] K. Autumn, A. M. Peattie, *Integr. Comp. Biol.* **2002**, *42*, 1081.
[12] E. Kroner, C. S. Davis, *J. Adhes.* **2015**, *91*, 481.
[13] G. Huber, H. Mantz, R. Spolenak, K. Mecke, K. Jacobs, S. N. Gorb, E. Arzt, *Proc. Natl. Acad. Sci. USA* **2005**, *102*, 16293.
[14] T. W. Kim, B. Bhushan, *J. R. Soc. Interface* **2008**, *5*, 319.
[15] A. Y. Stark, M. R. Klittich, M. Sitti, P. H. Niewiarowski, A. Dhinojwala, *Sci. Rep.* **2016**, *6*, 30936.
[16] U. Hiller, *Z. Morphol. Tiere* **1968**, *62*, 307.
[17] K. Autumn, N. Gravish, *Philos. Trans. A: Math. Phys. Eng. Sci.* **2008**, *366*, 1575.
[18] A. K. Geim, S. V. Dubonos, I. V. Grigorieva, K. S. Novoselov, A. A. Zhukov, S. Y. Shapoval, *Nat. Mater.* **2003**, *2*, 461.
[19] H. E. Jeong, J.-K. Lee, H. N. Kim, S. H. Moon, K. Y. Suh, *Proc. Natl. Acad. Sci. USA* **2009**, *106*, 5639.
[20] D. Paretkar, M. Kamperman, A. S. Schneider, D. Martina, C. Creton, E. Arzt, *Mater. Sci. Eng., C* **2011**, *31*, 1152.
[21] P. H. Niewiarowski, A. Y. Stark, A. Dhinojwala, *Bio-inspired Structured Adhesives*, Springer, Berlin **2017**, pp. 1–19.
[22] M. Zhou, Y. Tian, D. Sameoto, X. Zhang, Y. Meng, S. Wen, *ACS Appl. Mater. Interfaces* **2013**, *5*, 10137.
[23] J. Purtov, M. Frensemeier, E. Kroner, *ACS Appl. Mater. Interfaces* **2015**, *7*, 24127.
[24] S. Song, D.-M. Drotlef, C. Majidi, M. Sitti, *Proc. Natl. Acad. Sci. USA* **2017**, *114*, 201620344.
[25] C. Menon, Y. Li, D. Sameoto, C. Martens, *2008 2nd IEEE RAS EMBS International Conference on Biomedical Robotics and Biomechatronics*, IEEE, Piscataway, NJ **2008**, pp. 384–389.
[26] S. Kim, M. Spenko, S. Trujillo, B. Heyneman, D. Santos, M. R. Cutkosky, *IEEE Trans. Rob.* **2008**, *24*, 65.
[27] D. L. Christensen, E. W. Hawkes, S. A. Suresh, K. Ladenheim, M. R. Cutkosky, *2015 IEEE Int. Conf. on Robotics and Automation (ICRA)*, IEEE, Piscataway, NJ **2015**, pp. 4048–4055.
[28] E. W. Hawkes, D. L. Christensen, M. R. Cutkosky, *Proc. – IEEE Int. Conf. on Robotics and Automation*, IEEE, Piscataway, NJ **2015**, p. 3762.
[29] E. W. Hawkes, E. V. Eason, A. T. Asbeck, M. R. Cutkosky, *IEEE/ASME Trans. Mechatronics* **2013**, *18*, 518.
[30] J. Krahn, Y. Liu, A. Sadeghi, C. Menon, *Smart Mater. Struct.* **2011**, *20*, 115021.
[31] H. Jiang, E. W. Hawkes, V. Arutyunov, J. Tims, C. Fuller, J. P. King, C. Seubert, H. L. Chang, A. Parness, M. R. Cutkosky, *Proc. – IEEE Int. Conf. on Robotics and Automation*, IEEE, Piscataway, NJ **2015**, pp. 2828–2835.
[32] M. A. Estrada, B. Hockman, A. Bylard, E. W. Hawkes, M. R. Cutkosky, M. Pavone, *Proc. – IEEE Int. Conf. on Robotics and Automation*, IEEE, Piscataway, NJ **2016**, pp. 4907–4913.
[33] A. Wasay, D. Sameoto, *Lab Chip* **2015**, *15*, 2749.
[34] M. Zandvakili, M. M. Honari, P. Mousavi, D. Sameoto, *Adv. Mater. Technol.* **2017**, *2*, 1700144.

[35] M. F. Yanik, *Trends Biotechnol.* **2009**, *27*, 1.
[36] W. G. Bae, D. Kim, M. K. Kwak, L. Ha, S. M. Kang, K. Y. Suh, *Adv. Healthcare Mater.* **2013**, *2*, 109.
[37] M. K. Kwak, H.-E. E. Jeong, K. Y. Suh, *Adv. Mater.* **2011**, *23*, 3949.
[38] J. S. Kaiser, M. Kamperman, E. J. de Souza, B. Schick, E. Arzt, *Int. J. Artif. Organs* **2011**, *34*, 180.
[39] C. Greiner, A. Del Campo, E. Arzt, *Langmuir* **2007**, *23*, 3495.
[40] A. Del Campo, C. Greiner, E. Arzt, *Langmuir* **2007**, *23*, 10235.
[41] C.-Y. Hui, N. J. Glassmaker, T. Tang, A. Jagota, *J. R. Soc. Interface* **2004**, *1*, 35.
[42] M. Kamperman, E. Kroner, A. del Campo, R. M. McMeeking, E. Arzt, *Adv. Eng. Mater.* **2010**, *12*, 335.
[43] K. L. Johnson, K. Kendall, A. D. Roberts, *Proc. R. Soc., A: Math. Phys. Eng. Sci.* **1971**, *324*, 301.
[44] R. G. Beutel, S. N. Gorb, *J. Zool. Syst. Evol. Res.* **2001**, *39*, 177.
[45] J. M. R. Bullock, W. Federle, *Naturwissenschaften* **2011**, *98*, 381.
[46] R. Spolenak, S. Gorb, H. Gao, E. Arzt, *Proc. R. Soc. London, Ser. A* **2005**, *461*, 305.
[47] K. Kendall, *J. Phys. D: Appl. Phys.* **1971**, *4*, 1186.
[48] M. Barquins, D. Maugis, *J. Adhes.* **1981**, *13*, 53.
[49] D. Maugis, M. Barquins, *J. Phys. D: Appl. Phys.* **1983**, *16*, 1843.
[50] D. B. D. Bogy, *J. Appl. Mech.* **1971**, *38*, 377.
[51] A. R. Akisanya, N. A. Fleck, *Int. J. Solids Struct.* **1997**, *34*, 1645.
[52] S. N. Khaderi, N. A. Fleck, E. Arzt, R. M. McMeeking, *J. Mech. Phys. Solids* **2015**, *75*, 159.
[53] N. A. Fleck, S. N. Khaderi, R. M. McMeeking, E. Arzt, *J. Mech. Phys. Solids* **2017**, *101*, 30.
[54] R. M. McMeeking, E. Arzt, A. G. Evans, *J. Adhes.* **2008**, *84*, 675.
[55] T. Tang, C.-Y. Hui, N. J. Glassmaker, *J. R. Soc. Interface* **2005**, *2*, 505.
[56] K. N. G. Fuller, D. Tabor, *Proc. R. Soc. London, Ser. A* **1975**, *345*, 327.
[57] G. A. D. Briggs, B. J. Briscoe, *J. Phys. D: Appl. Phys.* **1977**, *10*, 2453.
[58] K. R. Shull, *Mater. Sci. Eng., R* **2002**, *36*, 1.
[59] C. Creton, M. Ciccotti, *Rep. Prog. Phys.* **2016**, *79*, 46601.
[60] J. Y. Chung, M. K. Chaudhury, *J. R. Soc. Interface* **2005**, *2*, 55.
[61] N. J. Glassmaker, A. Jagota, C.-Y. Hui, W. L. Noderer, M. K. Chaudhury, *Proc. Natl. Acad. Sci. USA* **2007**, *104*, 10786.
[62] W. L. Noderer, L. Shen, S. Vajpayee, N. J. Glassmaker, A. Jagota, C.-Y. Hui, *Proc. R. Soc. London, Ser. A* **2007**, *463*, 2631.
[63] E. P. Arul, A. Ghatak, *Langmuir* **2012**, *28*, 4339.
[64] R. Spolenak, S. Gorb, E. Arzt, *Acta Biomater.* **2005**, *1*, 5.
[65] C. Greiner, R. Spolenak, E. Arzt, *Acta Biomater.* **2009**, *5*, 597.
[66] B. N. J. Persson, S. Gorb, *J. Chem. Phys.* **2003**, *119*, 11437.
[67] B. N. J. Persson, *J. Chem. Phys.* **2003**, *118*, 7614.
[68] V. Barreau, R. Hensel, N. K. Guimard, A. Ghatak, R. M. McMeeking, E. Arzt, *Adv. Funct. Mater. Mater.* **2016**, *26*, 4687.
[69] S. N. Gorb, A. E. Filippov, *Beilstein J. Nanotechnol.* **2014**, *5*, 837.
[70] C. T. Bauer, E. Kroner, N. A. Fleck, E. Arzt, *Bioinspir. Biomim.* **2015**, *10*, 66002.
[71] W. R. Hansen, K. Autumn, *Proc. Natl. Acad. Sci. USA* **2005**, *102*, 385.
[72] C. J. Clemente, J. M. R. Bullock, A. Beale, W. Federle, *J. Exp. Biol.* **2010**, *213*, 635.
[73] C. Hui, L. Shen, A. Jagota, K. Autumn, *Proc. of the 29th Annual Meeting of the Adhesion Society*, Adhesion Society, Jacksonville, FL **2006**, pp. 29–31.
[74] S. Gorb, M. Varenberg, A. Peressadko, J. Tuma, *J. R. Soc. Interface* **2007**, *4*, 271.
[75] S. Gorb, *Attachment Devices of Insect Cuticle*, Springer Science & Business Media, Berlin **2001**.
[76] S. N. Gorb, M. Varenberg, *J. Adhes. Sci. Technol.* **2007**, *21*, 1175.
[77] A. Del Campo, C. Greiner, I. Álvarez, E. Arzt, *Adv. Mater.* **2007**, *19*, 1973.
[78] S. Kim, M. Sitti, *Appl. Phys. Lett.* **2006**, *89*, 261911.
[79] L. Heepe, a. E. Kovalev, M. Varenberg, J. Tuma, S. N. Gorb, *Theor. Appl. Mech. Lett.* **2012**, *2*, 14008.
[80] E. Kroner, E. Arzt, *Int. J. Adhes. Adhes.* **2012**, *36*, 32.
[81] L. Heepe, A. E. Kovalev, A. E. Filippov, S. N. Gorb, *Phys. Rev. Lett.* **2013**, *111*, 104301.
[82] E. P. Chan, C. Greiner, E. Arzt, A. J. Crosby, *MRS Bull.* **2007**, *32*, 496.
[83] A. Del Campo, E. Arzt, *Macromol. Biosci.* **2007**, *7*, 118.
[84] C. Greiner, *Biomimetic and Bioinspired Nanomaterials*, Vol. *7*, Wiley-VCH, Weinheim, Germany **2010**, pp. 1–39.
[85] C. K. Hossfeld, A. S. Schneider, E. Arzt, C. P. Frick, *Langmuir* **2013**, *29*, 15394.
[86] A. V. Spuskanyuk, R. M. McMeeking, V. S. Deshpande, E. Arzt, *Acta Biomater.* **2008**, *4*, 1669.
[87] R. G. Balijepalli, M. R. Begley, N. A. Fleck, R. M. McMeeking, E. Arzt, *Int. J. Solids Struct.* **2016**, *85*, 160.
[88] B. Aksak, K. Sahin, M. Sitti, *Beilstein J. Nanotechnol.* **2014**, *5*, 630.
[89] G. Carbone, E. Pierro, *Small* **2012**, *8*, 1449.
[90] J. Fischer, M. Wegener, *Laser Photonics Rev.* **2013**, *7*, 22.
[91] S. C. L. Fischer, K. Groß, O. Torrents Abad, M. M. Becker, E. Park, R. Hensel, E. Arzt, *Adv. Mater. Interfaces* **2017**, *4*, 1700292.
[92] H. Peisker, J. Michels, S. N. Gorb, *Nat. Commun.* **2013**, *4*, 1661.
[93] I. Scholz, W. Baumgartner, W. Federle, *J. Comp. Physiol., A* **2008**, *194*, 373.
[94] M. P. Murphy, B. Aksak, M. Sitti, *J. Adhes. Sci. Technol.* **2007**, *21*, 1281.
[95] H. K. Minsky, K. T. Turner, *Appl. Phys. Lett.* **2015**, *106*, 201604.
[96] H. K. Minsky, K. T. Turner, *ACS Appl. Mater. Interfaces* **2017**, *9*, 18322.
[97] R. G. Balijepalli, S. C. L. L. Fischer, R. Hensel, R. M. McMeeking, E. Arzt, *J. Mech. Phys. Solids* **2017**, *99*, 357.
[98] S. C. L. Fischer, E. Arzt, R. Hensel, *ACS Appl. Mater. Interfaces* **2017**, *9*, 1036.
[99] R. Hensel, R. M. McMeeking, A. Kossa, *J. Adhes.* **2018**, https://doi.org/10.1080/00218464.2017.1381603.
[100] R. E. Webber, K. R. Shull, A. Roos, C. Creton, *Phys. Rev. E* **2003**, *68*, 21805.
[101] M. Zhou, N. Pesika, H. Zeng, Y. Tian, J. Israelachvili, *Friction* **2013**, *1*, 114.
[102] D. Labonte, W. Federle, *Philos. Trans. R. Soc., B* **2015**, *370*, 20140027.
[103] K. Autumn, P. H. Niewiarowski, J. B. Puthoff, *Annu. Rev. Ecol. Evol. Syst.* **2014**, *45*, 445.
[104] Y. Tian, N. Pesika, H. Zeng, K. Rosenberg, B. Zhao, P. McGuiggan, K. Autumn, J. Israelachvili, *Proc. Natl. Acad. Sci. USA* **2006**, *103*, 19320.
[105] M. P. Murphy, B. Aksak, M. Sitti, *Small* **2009**, *5*, 170.
[106] K. Jin, Y. Tian, J. S. Erickson, J. Puthoff, K. Autumn, N. S. Pesika, *Langmuir* **2012**, *28*, 5737.
[107] P. Day, E. V. Eason, N. Esparza, D. Christensen, M. Cutkosky, *J. Micro Nano-Manufacturing* **2013**, *1*, 11001.
[108] K. Jin, J. C. Cremaldi, J. S. Erickson, Y. Tian, J. N. Israelachvili, N. S. Pesika, *Adv. Funct. Mater.* **2014**, *24*, 574.
[109] M. K. Kwak, H. E. Jeong, W. G. Bae, H. S. Jung, K. Y. Suh, *Small* **2011**, *7*, 2296.
[110] J. Tamelier, S. Chary, K. L. Turner, *Langmuir* **2012**, *28*, 8746.
[111] J. Lee, S. Seo, J. Lee, K. S. Kim, K. H. Ko, J. H. Lee, *ACS Appl. Mater. Interfaces* **2014**, *6*, 1345.
[112] L. Xue, J. Iturri, M. Kappl, H. J. Butt, A. Del Campo, *Langmuir* **2014**, *30*, 11175.
[113] D. Sameoto, C. Menon, *J. Micromech. Microeng.* **2009**, *19*, 115026.
[114] W. Bin Khaled, D. Sameoto, *Bioinspir. Biomim.* **2013**, *8*, 44002.

[115] Y. Wang, H. Tian, J. Shao, D. Sameoto, X. Li, L. Wang, H. Hu, Y. Ding, B. Lu, *ACS Appl. Mater. Interfaces* **2016**, *8*, 10029.
[116] Y. Li, J. Krahn, C. Menon, *J. Bionic Eng.* **2016**, *13*, 181.
[117] H. Jiang, E. W. Hawkes, C. Fuller, M. A. Estrada, S. A. Suresh, N. Abcouwer, A. K. Han, S. Wang, C. J. Ploch, A. Parness, M. R. Cutkosky, *Sci. Rob.* **2017**, *2*, 1.
[118] Y. Li, A. Ahmed, D. Sameoto, C. Menon, *Robotica* **2012**, *30*, 79.
[119] M. Henrey, A. Ahmed, P. Boscariol, L. Shannon, C. Menon, *J. Bionic Eng.* **2014**, *11*, 1.
[120] K. Liew, H. Shahsavan, B. Zhao, *Int. J. Adhes. Adhes.* **2017**, *76*, 47.
[121] J. Jeong, J. Kim, K. Song, K. Autumn, J. Lee, *J. R. Soc. Interface* **2014**, *11*, 20140627.
[122] E. W. Hawkes, D. L. Christensen, A. K. Han, H. Jiang, M. R. Cutkosky, *Proc. –IEEE Int. Conf. on Robotics and Automation*, IEEE, Piscataway, NJ **2015**, pp. 2305–2312.
[123] S. Song, M. Sitti, *Adv. Mater.* **2014**, *26*, 4901.
[124] M. Varenberg, S. Gorb, *J. R. Soc. Interface* **2008**, *5*, 785.
[125] D. Paretkar, M. Kamperman, D. Martina, J. Zhao, C. Creton, A. Lindner, A. Jagota, R. McMeeking, E. Arzt, *J. R. Soc. Interface* **2013**, *10*, 20130171.
[126] D. Paretkar, A. S. Schneider, E. Kroner, E. Arzt, *MRS Commun.* **2011**, *1*, 53.
[127] S. Stark, M. R. Begley, R. M. McMeeking, *J. Appl. Mech.* **2012**, *80*, 1.
[128] P. Y. Isla, E. Kroner, *Adv. Funct. Mater.* **2015**, *25*, 2444.
[129] S. Reddy, E. Arzt, A. Del Campo, *Adv. Mater.* **2007**, *19*, 3833.
[130] J. D. Eisenhaure, T. Xie, S. Varghese, S. Kim, *ACS Appl. Mater. Interfaces* **2013**, *5*, 7714.
[131] M. Frensemeier, J. S. Kaiser, C. P. Frick, A. S. Schneider, E. Arzt, R. S. Fertig, E. Kroner, *Adv. Funct. Mater.* **2015**, *25*, 3013.
[132] M. T. Northen, C. Greiner, E. Arzt, K. L. Turner, *Adv. Mater.* **2008**, *20*, 3905.
[133] J. Cui, D. M. Drotlef, I. Larraza, J. P. Fernández-Blázquez, L. F. Boesel, C. Ohm, M. Mezger, R. Zentel, A. Del Campo, *Adv. Mater.* **2012**, *24*, 4601.
[134] D. M. Drotlef, P. Blümler, A. Del Campo, *Adv. Mater.* **2014**, *26*, 775.
[135] E. Kizilkan, J. Strueben, A. Staubitz, S. N. Gorb, *Sci. Rob.* **2017**, *2*, eaak9454.
[136] E. Kroner, R. Maboudian, E. Arzt, *Adv. Eng. Mater.* **2010**, *12*, 398.
[137] C. A. Dahlquist, *Treatise Adhes. Adhes.* **1969**, *2*, 219.
[138] J. Davies, S. Haq, T. Hawke, J. P. Sargent, *Int. J. Adhes. Adhes.* **2009**, *29*, 380.
[139] A. Asbeck, S. Dastoor, A. Parness, L. Fullerton, N. Esparza, D. Soto, B. Heyneman, M. Cutkosky, *Proc. – IEEE Int. Conf. on Robotics and Automation*, IEEE, Piscataway, NJ **2009**, pp. 2675–2680.
[140] S. Vajpayee, A. Jagota, C.-Y. Hui, *J. Adhes.* **2010**, *86*, 39.
[141] N. Cañas, M. Kamperman, B. Völker, E. Kroner, R. M. McMeeking, E. Arzt, *Acta Biomater.* **2012**, *8*, 282.
[142] C.-Y. Hui, N. J. Glassmaker, A. Jagota, *J. Adhes.* **2005**, *81*, 699.
[143] H. Kasem, M. Varenberg, *J. R. Soc. Interface* **2013**, *10*, 20130620.
[144] D. R. King, M. D. Bartlett, C. A. Gilman, D. J. Irschick, A. J. Crosby, *Adv. Mater.* **2014**, *26*, 4345.
[145] F. W. DelRio, M. P. de Boer, J. A. Knapp, E. David Reedy, P. J. Clews, M. L. Dunn, *Nat. Mater.* **2005**, *4*, 629.
[146] W. B. Dapp, A. Lücke, B. N. J. Persson, M. H. Müser, *Phys. Rev. Lett.* **2012**, *108*, 1.
[147] L. Pastewka, M. O. Robbins, *Proc. Natl. Acad. Sci. USA* **2014**, *111*, 3298.
[148] M. H. Müser, *Tribol. Int.* **2016**, *100*, 41.
[149] B. N. J. Persson, *Surf. Sci. Rep.* **2006**, *61*, 201.
[150] A. W. Bush, R. D. Gibson, T. R. Thomas, *Wear* **1975**, *35*, 87.
[151] J. A. Greenwood, J. B. P. Williamson, *Proc. R. Soc. London, Ser. A* **1966**, *295*, 300.
[152] R. M. McMeeking, L. Ma, E. Arzt, *Adv. Eng. Mater.* **2010**, *12*, 389.
[153] B. N. J. Persson, O. Albohr, C. Creton, V. Peveri, *J. Chem. Phys.* **2004**, *120*, 8779.
[154] C. Créton, L. Leibler, *J. Polym. Sci., Part B: Polym. Phys.* **1996**, *34*, 545.
[155] T. D. B. Jacobs, T. Junge, L. Pastewka, *Surf. Topogr. Metrol. Prop.* **2017**, *5*, 13001.
[156] B. N. J. Persson, *J. Chem. Phys.* **2001**, *115*, 3840.
[157] B. N. J. Persson, *Phys. Rev. Lett.* **2001**, *87*, 116101.
[158] S. Akarapu, T. Sharp, M. O. Robbins, *Phys. Rev. Lett.* **2011**, *106*.
[159] R. Pohrt, V. L. Popov, *Phys. Rev. Lett.* **2012**, *108*, 104301.
[160] E. Turi, *Thermal Characterization of Polymeric Materials*, Elsevier, San Diego, CA **2012**.
[161] A. Zosel, *Colloid Polym. Sci.* **1985**, *263*, 541.
[162] A. Zosel, *J. Adhes.* **1991**, *34*, 201.
[163] G. Castellanos, E. Arzt, M. Kamperman, *Langmuir* **2011**, *27*, 7752.
[164] N. Lakhera, A. Graucob, A. S. Schneider, E. Kroner, M. Micciché, E. Arzt, C. P. Frick, *MRS Commun.* **2013**, *3*, 73.
[165] H. Yu, Z. Li, Q. Jane Wang, *Mech. Mater.* **2013**, *60*, 55.
[166] V. Barreau, D. Yu, R. Hensel, E. Arzt, *J. Mech. Behav. Biomed. Mater.* **2017**, *76*, 110.
[167] S. H. Lee, S. W. Kim, B. S. Kang, P.-S. Chang, M. K. Kwak, *Soft Matter* **2018**, *14*, 2586.
[168] H. Yi, I. Hwang, J. H. Lee, D. Lee, H. Lim, D. Tahk, M. Sung, W. G. Bae, S. J. Choi, M. K. Kwak, H. E. Jeong, *ACS Appl. Mater. Interfaces* **2014**, *6*, 14590.
[169] M. R. Cutkosky, *Interface* **2015**, *5*, 20150015.